Frontogenesis in the Presence of Small Stability to Slantwise Convection

A. J. THORPE

Department of Meteorology, University of Reading, Reading, England

K. A. EMANUEL

Center for Meteorology and Physical Oceanography, Massachusetts Institute of Technology, Cambridge, MA 02139

(Manuscript received 5 November 1984, in final form 18 March 1985)

ABSTRACT

It is often observed that, despite the existence of near neutrality to slantwise convection, rainbands and snowbands can persist for long periods with narrow intense updrafts producing large quantities of precipitation in many cases. This is probably due to the presence of active frontogenesis which, as shown here, maintains such structures.

In order to investigate this process, we use two-dimensional semigeostrophic theory to solve the deformation-forced frontogenesis problem for a circumstance in which the stability to moist slantwise convection is small but positive. In this case, numerical simulation is necessary to determine the evolution of the front. Several previous studies have described the role of diabatic forcing in modifying the cross-frontal circulation by use of the Sawyer–Eliassen equation. In particular, analytic solutions of that equation for the case of small moist symmetric stability show that a narrow updraft should occur ahead of the maximum geostrophic frontogenesis.

Numerical solutions to the time-dependent problem are described in this paper; it is apparent that the latent heat release produces significant sources and sinks of potential vorticity which lead to a sharp increase in the rate of surface frontogenesis. As shown by previous diagnostic solutions, the scale of the ascent is considerably reduced and there is descent at midlevels in the frontal region where ascent would occur in the absence of condensation. However, the surface maxima of vorticity and ageostrophic convergence are only slightly displaced toward the warm air. Due to the increased rate of frontogenesis and the local variations in potential vorticity, the geostrophic flow is weakly modified.

The variations in potential vorticity along isentropes produced by the slantwise convection could lead to the growth of a (secondary) internal baroclinic/barotropic instability, which may explain the tendency for frontal precipitation bands to become wavelike in the "along-front" direction. Such an instability cannot be described in the present two-dimensional numerical model but should be investigated further using a more appropriate model.

It is also shown that the growth of the baroclinic wave in which such frontogenesis is assumed to occur is increased by the presence of the diabatic forcing. This is done by solving the Eady problem assuming small stability to slantwise convection. In addition to an increased growth rate, the wave of maximum growth has a smaller horizontal scale.

1. Introduction

In regions of the atmosphere in which the air is lifted to saturation and the gradient of equivalent (or wet-bulb) potential temperature in a vertical sounding is negative, upright convection can occur. This unstable condensation takes place on a typical horizontal scale on the order of the depth of the unstable layer, and as such cannot be represented explicitly in large-scale models. A common parameterization scheme involves adjusting the lapse rate in the unstable column back to one of moist-neutrality. It is arguable whether this is an adequate representation of the conditions observed after the passage of a convective storm, since the atmosphere is then often found to be somewhat stable to further upright convection. Surface fluxes of heat and moisture or horizontal advection are necessary to destabilize the atmosphere if further upright convection is to occur. However, there are many situations in the atmosphere when the vertical sounding is stable to moist adiabatic displacements but there is significant cloud and precipitation. Such cases are frequently referred to as stable or nonconvective condensation and are characterized by a saturated layer but a stable sounding. These situations are accounted for in models by formulating equations to describe condensation on the scale of a grid length ($\sim$150 km) or greater (e.g., Sundqvist, 1978).

However, it is becoming apparent that there are well-defined situations in which, despite the existence of stability to upright convection, the atmosphere produces significant structure on the scale of 100 km or less. Bennetts and Hoskins (1979), Emanuel (1983a,b) and others have postulated that some of these events

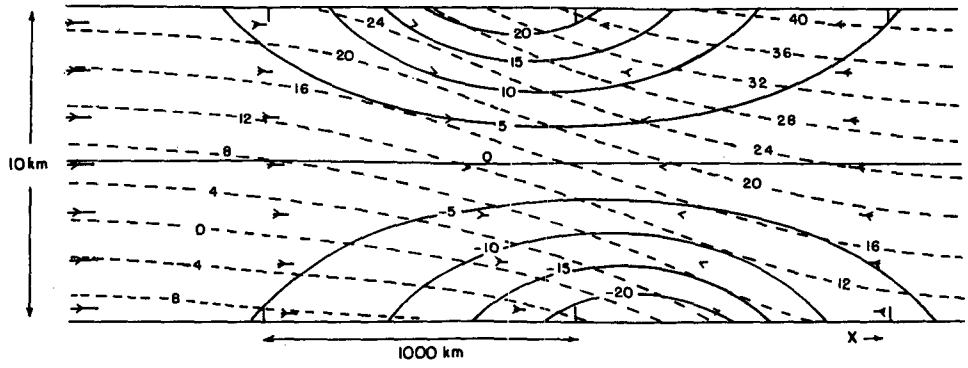

FIG. 1a. Cross section in the x–z plane showing the initial distribution of long-front velocity (m s^{-1}; solid), potential temperature perturbation (°C; dashed) and total velocity projected onto the x–z plane (arrows). A vertical length of the arrows equivalent to 1 km represents a vertical velocity of 10 cm s^{-1}, while a horizontal length equivalent to 100 km represents a horizontal velocity of 10 m s^{-1}.

are examples of slantwise moist convection which is driven by a combination of gravitational and centrifugal buoyancy, and for which a necessary condition for instability is negative equivalent potential vorticity. A straightforward analogue to the parcel method of assessing convective instability using tephigrams was developed by Emanuel (1983a), who showed that stability can be assessed by lifting parcels adiabatically along surfaces of constant M, where $M = V + fx$, V is the component of geostrophic wind along isotherms, and x is the coordinate along the temperature gradient. These surfaces are vertical in regions where there is no vertical wind shear but make a small angle to the horizontal in strong baroclinic zones. It is possible for an atmosphere which is stable to upright convection to be unstable to slantwise convection, and likewise if the atmosphere has undergone an adjustment to vertical neutrality by upright convection it may still be unstable to slantwise convection.

Detailed case studies of slantwise convective storms indicate that a condition of near neutrality to moist adiabatic displacement along M-surfaces is characteristic (Emanuel, 1983b; Sanders and Bosart, 1985). This suggests that an appropriate way to include the effects of slantwise convection in large-scale models is to make some form of moist-adiabatic adjustment (in the manner of Betts, 1983, perhaps) along M-surfaces. These surfaces are perforce upright in a geostrophic coordinate system and the adjustment is thus similar in these coordinates to that for upright convection.

In contrast to upright convection, it is observed that structures characteristic of slantwise convection can persist even after a condition of near neutrality has been achieved. These situations appear to be characterized by frontogenetical forcing, (Sanders and Bosart, 1985; Emanuel, 1985). It is this circumstance which will be examined in some detail in this paper. The development of the state in which there is neutrality to slantwise convection in the presence of frontogenesis is not considered here but represents an important dynamical problem. Little is known about the growth of instabilities in a region subject to forcing, analytical approaches being complicated by the existence of a hyperbolic region (containing the instability) embedded

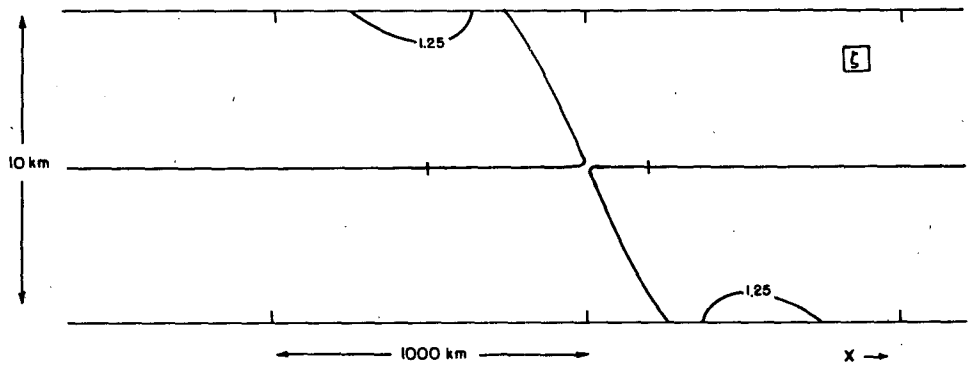

FIG. 1b. Cross section of initial values of the vertical component of absolute vorticity (10^{-4} s^{-1}). The maximum and minimum values of vorticity are 1.4×10^{-4} s^{-1} and 0.77×10^{-4} s^{-1}, respectively.

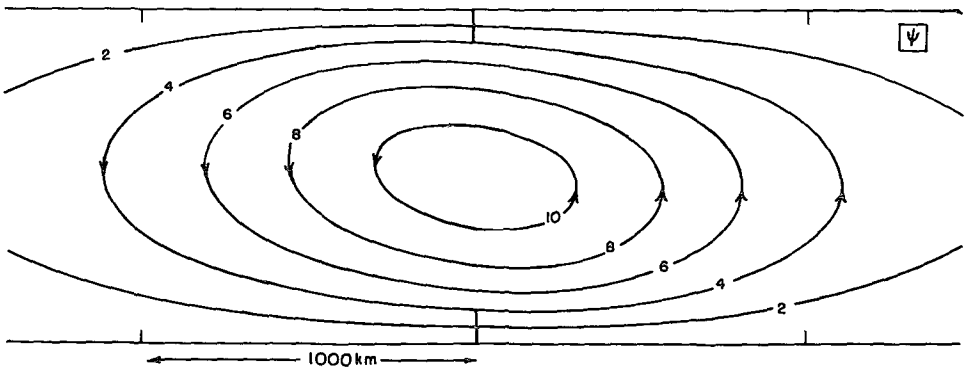

FIG. 1c. Cross section of initial streamfunction (10^3 kg m^{-1} s^{-1}). The maximum value of ψ is 11023 kg m^{-1} s^{-1}.

within an elliptic region (of stable forced motion). This problem is one in which numerical modeling should play an important part.

Several previous studies have been made of frontal circulations including diabatic forcing typical of latent heat release. In the first, by Sawyer (1956), a diabatic source term was included in what is now known as the Sawyer–Eliassen equation for the cross-frontal circulation. In that study a prescribed region of heating was included to represent the effects of a specified moisture distribution. Subsequent similar work by Thorpe and Nash (1984) included a parameterization of upright convection dependent on the ageostrophic low-level convergence. They found that with such a scheme the heating becomes decoupled from the local vertical velocity and a narrow updraft develops ahead of the front, with descent on either side. In this way it is possible for a definite scale of the frontal rainband to develop; evidence for this structure of the descent is apparent in the observations shown in Sanders and Bosart (1985). Even so, the above-mentioned observations indicate that in many frontal zones, the air is stable to upright convection and nearly neutral to slantwise convection. The response to frontogenetical forcing of an atmosphere which is nearly neutral to saturated slantwise displacements has been considered recently by Emanuel (1985), henceforth referred to as E85. He solved the semigeostrophic form of the Sawyer–Eliassen equation for prescribed frontogenetical forcing, and allowed the potential vorticity (which acts like static stability in this case) to take on one value where the motion is downward and another, much smaller value, in rising air. E85 found that the updraft in the warm air becomes very narrow and is displaced ahead of its position in the absence of heating. Consequently, he speculated that the diabatic forcing may decrease the frontogenesis, as there was descent in the region of maximum surface geostrophic forcing.

These diagnostic studies are incomplete in that no allowance is made for the change in the geostrophic state due to the latent heating. To determine a more complete description of this problem, a time-dependent semigeostrophic frontogenesis model is used here to describe the evolution of a front in a moist atmosphere which is nearly neutral to slantwise convection. Several other authors have made time dependent simulations of moist frontogenesis, including Ross and Orlanski (1978), Williams *et al.* (1981), and more recently Hsie *et al.* (1984).[1] These models have attempted to include unstable moist processes using complicated parameterization schemes. However, it is difficult to extract dynamical principles concerning the role of moisture from these simulations, for a variety of reasons. For example Ross and Orlanski (1978) and Hsie *et al.* (1984) examine the problem of shear-forced frontogenesis, and have a moist initial state which is unstable to upright convection. The aim in this paper is to use the simplest possible condensation scheme consistent with conservation of θ_e in a model which highlights the dynamical structure of fronts. In contrast to earlier studies, we specifically choose conditions which are always stable (though weakly so) to moist convection.

We proceed with a concise description of the relevant equations and of the numerical model. Section 3 describes some simple deductions about the role of condensation in the frontogenesis problem using a scale analysis of the equations. In Section 4 a detailed comparison of frontogenesis in the dry and moist cases is presented including a description of the variation of the essential features of the evolution with the value of the equivalent potential vorticity. The paper finishes with a discussion which includes a description of further work needed to clarify some of the questions raised by the present results.

2. Semigeostrophic formulation

The semigeostrophic theory of frontogenesis has been reviewed by Hoskins (1982) and a more or less

[1] The latter paper was published after the submission of this paper.

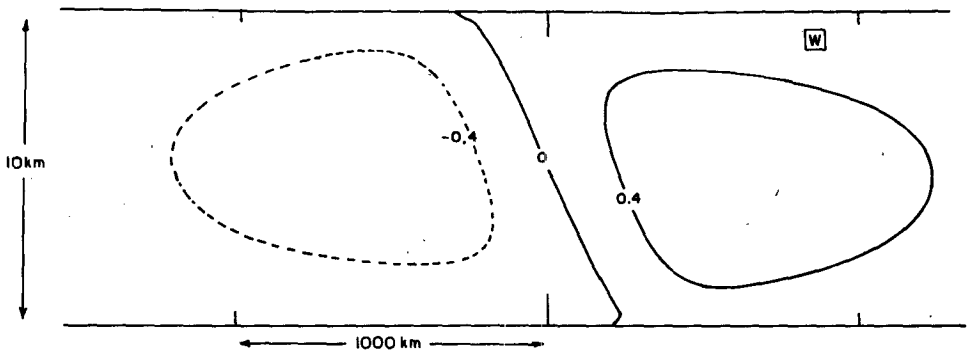

FIG. 1d. Cross section of initial vertical velocity (cm s^{-1}). The minimum and maximum values of w are 0.68 cm s^{-1} and -0.68 cm s^{-1}, respectively.

complete description of the dry problem has been deduced. In this paper we use the simplest frontogenesis model, in which there is initially uniform potential vorticity with a specified horizontal temperature gradient on the two horizontal boundaries. Frontogenesis is produced by a constant deformation field and, in the absence of moisture, analytical solutions can be obtained for the collapse to a discontinuity (Hoskins and Bretherton, 1972). The effects of moisture will be represented by a diabatic source consistent with the conservation of equivalent potential vorticity q_e in saturated regions. Furthermore, it will be assumed that the atmosphere has already undergone adjustment, by slantwise convection, to a state of small stability to slantwise displacements. This is equivalent to making q_e small. We take this to be the simplest treatment of condensation and latent heat release which captures the fundamental physics of the observed phenomenon.

The derivation of the following equations can be found in Hoskins and Bretherton (1972); they describe two-dimensional semigeostrophic dynamics using the geostrophic coordinate transformation. The new coordinates are defined as:

$$X \equiv x + V/f, \quad Z \equiv z, \quad T \equiv t,$$

where V is the geostrophic flow along the front.

The total flow (suffix T) is composed of a deformation field with amplitude 2α and ageostrophic velocities (lower case):

$$U_T = -\alpha x + u, \quad V_T = \alpha y + V, \quad W = w.$$

The thermal wind balance can be written as:

$$\frac{\partial V}{\partial Z} = \frac{g}{f\theta_0}\frac{\partial \theta}{\partial X}.$$

The basic equations to be solved are for the potential vorticity, the ageostrophic streamfunction, and the modified geopotential function:

$$\frac{dq}{dT} = \frac{\zeta}{\rho}\frac{\partial S}{\partial Z}, \tag{1}$$

$$\rho\frac{\partial}{\partial Z}\left(\frac{1}{\rho}\frac{\partial \psi}{\partial Z}\right) + \frac{\partial}{\partial X}\left(\rho q \frac{g}{f^3\theta_0}\frac{\partial \psi}{\partial X}\right) = -2Q - \frac{g\rho}{f^3\theta_0}\frac{\partial S}{\partial X}, \tag{2}$$

$$\frac{\partial^2 \Phi}{\partial X^2} + \frac{\theta_0 f^3}{g\rho q}\frac{\partial^2 \Phi}{\partial Z^2} = f^2, \tag{3}$$

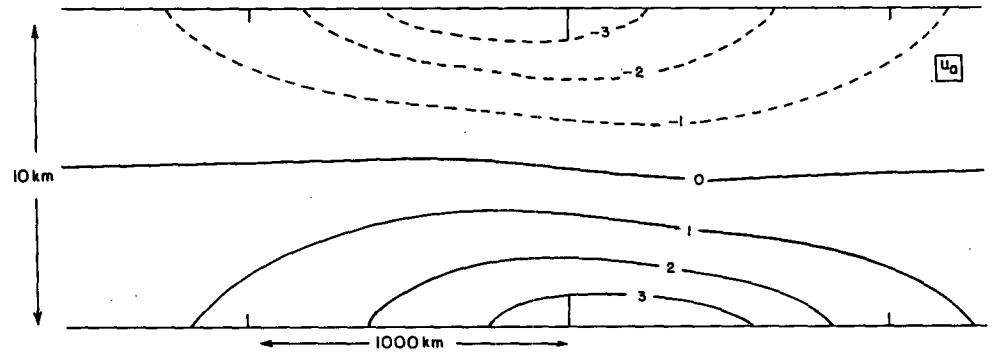

FIG. 1e. Cross section of initial ageostrophic velocity in the x direction (m s^{-1}). The maximum and minimum values are 4 m s^{-1} and -4 m s^{-1}, respectively.

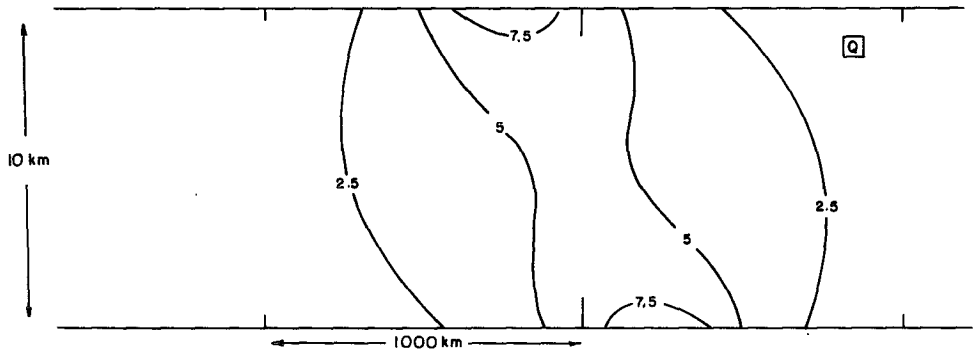

FIG. 1f. Initial geostrophic forcing (10^{-4} kg m^{-3} s^{-1}); $Q_{max} = 9 \times 10^{-4}$ kg m^{-3} s^{-1}.

where

$$q = \frac{\zeta}{\rho}\frac{\partial \theta}{\partial Z},$$

$$\zeta = f\Big/\left(1 - f^{-1}\frac{\partial V}{\partial X}\right),$$

$$\Phi \equiv \varphi + \frac{1}{2}V^2,$$

$$u = \frac{1}{\rho}\frac{\partial \psi}{\partial z},$$

$$V = \frac{1}{f}\frac{\partial \Phi}{\partial X},$$

$$w = -\frac{1}{\rho}\frac{\zeta}{f}\frac{\partial \psi}{\partial X},$$

$$\theta = \frac{\theta_0}{g}\frac{\partial \Phi}{\partial Z},$$

$$\frac{d\theta}{dT} = S,$$

$$Q = \rho\frac{\alpha}{f}\frac{\partial V}{\partial Z}.$$

Here φ is the geopotential, ζ the absolute vorticity, ρ the density, θ the potential temperature, and Q the geostrophic forcing of frontogenesis.

The diabatic source term S produces sources and sinks of potential vorticity, but it cannot change the volume average potential vorticity if there is no heating of the boundaries. Consider the volume integral of the potential vorticity equation (1) in physical coordinates:

$$\frac{\partial I}{\partial t} = \int\int \frac{\zeta}{\rho}\frac{\partial S}{\partial Z}\,dxdz,$$

where

$$I \equiv \int\int q dxdz.$$

Here we have assumed zero total boundary flux of q. Transforming to geostrophic coordinates, using the Jacobian of the transformation, gives:

$$\frac{\partial I}{\partial T} = \int\int \frac{f}{\rho}\frac{\partial S}{\partial Z}\,dXdZ$$

$$= \int \frac{f}{\rho}(S_t - S_b)dX.$$

Here t and b refer to top and bottom boundaries, respectively. Thus I is a constant given that there is no

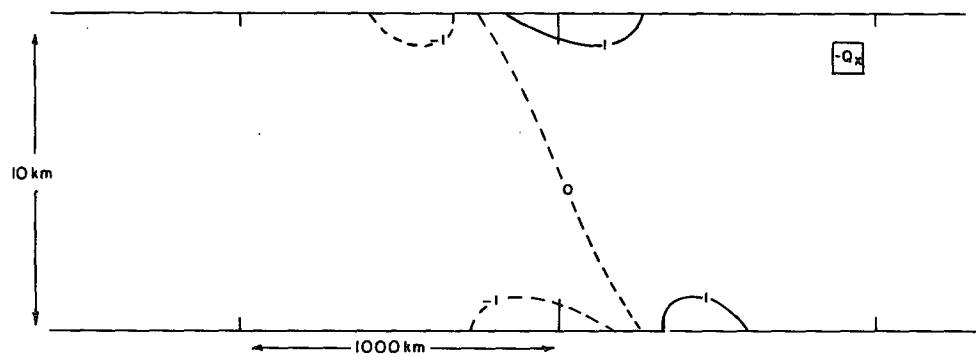

FIG. 1g. The x-derivative of geostrophic forcing (10^{-9} kg m^{-4} s^{-1}); $-Q_{xmax} = 1.6 \times 10^{-9}$ kg m^{-4} s^{-1}; $-Q_{xmin} = -1.6 \times 10^{-9}$ kg m^{-4} s^{-1}.

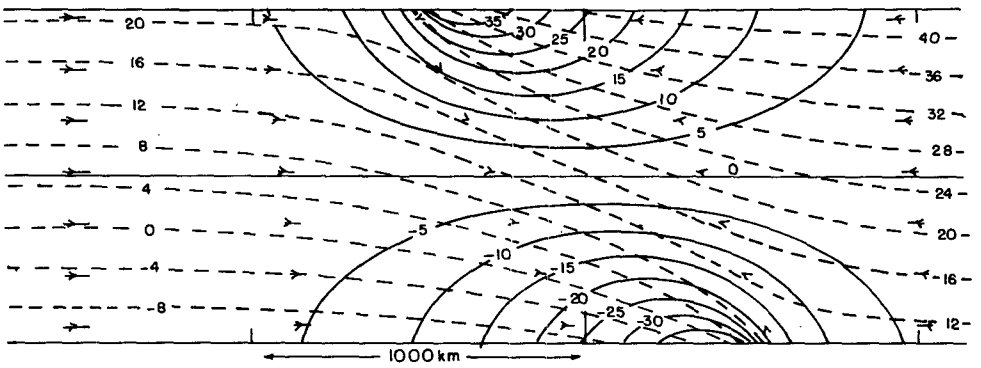

FIG. 2a. As in Fig. 1a but after 1 day of the dry simulation; $V_{max} = 41.4$ m s^{-1}; $V_{min} = -41.4$ m s^{-1}.

diabatic forcing on the horizontal boundaries. (Using the boundary variations of potential temperature described below gives $I = q_0 A$, where A is the domain area and q_0 is the potential vorticity remote from the frontal zone.)

Once the form of S has been deduced, the time integration proceeds by integrating the potential vorticity forward in time, then determining the new potential function (which gives the new V and hence Q), and finally solving for the ageostrophic streamfunction. The vertical velocity is then available for the calculation of the advection term in the potential vorticity equation. The numerical schemes used are simple leapfrog for q and an elliptic equation solver involving Gauss–Seidel reduction in one dimension and a fast Fourier transform method in the other (details can be found in Heckley, 1980).

The elliptic equations for ψ and Φ require boundary conditions, which we specify in the following form:

$$\psi = 0$$

on all boundaries ($u = 0$ on lateral boundaries and $w = 0$ on horizontal boundaries),

$$\Phi_z = \frac{g}{\theta_0}\frac{2\Delta\theta}{\pi}\tan^{-1}(X/L)$$

on bottom boundary,

$$\Phi_z = \frac{g}{\theta_0}\left[\frac{2\Delta\theta}{\pi}\tan^{-1}(X/L) + \frac{\rho q_0 Z}{f}\right]$$

on top boundary,

$$\Phi = g\frac{\Delta\theta}{\theta_0}(Z - H/2) + \frac{g\rho q_0}{\theta_0 f}\frac{Z^2}{2}$$

on right lateral boundary, and

$$\Phi = -g\frac{\Delta\theta}{\theta_0}(Z - H/2) + \frac{g\rho q_0}{\theta_0 f}\frac{Z^2}{2}$$

on left lateral boundary.

The conditions on Φ are actually a specification of θ on all boundaries, and this case represents a circumstance in which the horizontal temperature gradient is initially greatest in the middle of the domain. On the horizontal boundaries, which are material surfaces, there is no diabatic forcing and so it is easy to show that the θ distribution there is as given above with $L = L_0 \exp(-\alpha T)$. On the vertical boundaries the θ-profile of constant lapse rate can be integrated to give conditions on Φ up to an arbitrary constant. This constant for Φ is fixed by demanding that the volume integral of V is zero, which corresponds to forcing an atmo-

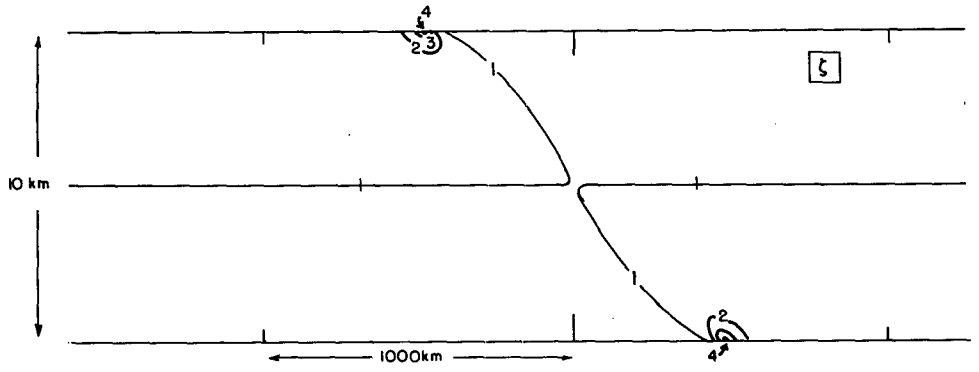

FIG. 2b. As in Fig. 1b but after 1 day of the dry simulation; $\zeta_{max} = 4.6 \times 10^{-4}$ s^{-1}; $\zeta_{min} = 0.56 \times 10^{-4}$ s^{-1}.

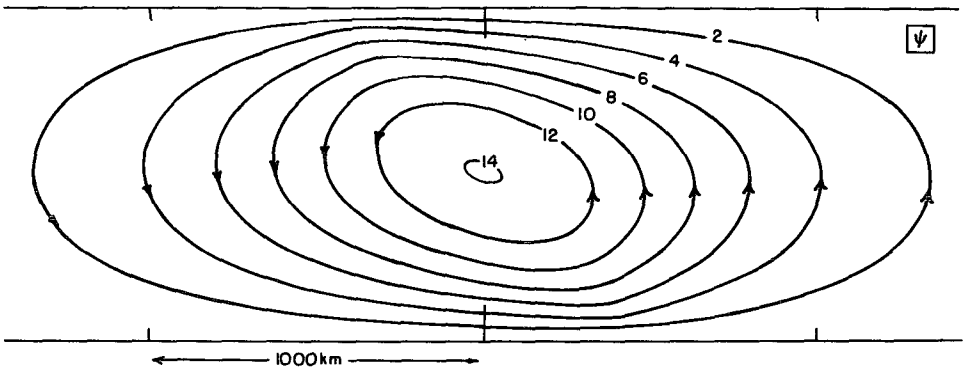

FIG. 2c. As in Fig. 1c but after 1 day of the dry simulation; $\psi_{max} = 14058$ kg m^{-1} s^{-1}.

sphere with negligible V at large time in the past, and is implemented by requiring the integral of Φ with respect to z to be the same on both lateral boundaries. For all the simulations to be described here the "initial" values of L and q, and the value of $\Delta\theta$ are:

$$L_0 = 350 \text{ km}, \quad q_0 = 2.67 \times 10^{-7} \text{ m}^2 \text{ s}^{-1} \text{ K kg}^{-1},$$
$$\Delta\theta = 12 \text{ K}.$$

Note that this is the state after a period of (dry) frontogenesis has already taken place. The numerical model domain is 5000 km by 10 km with grid lengths in geostrophic coordinates of 39 km and 256 m. In the vicinity of the front, the horizontal grid length in physical space becomes considerably smaller and at the time of frontal collapse it is zero.

As has already been mentioned, the diabatic term will be deduced from the condition that the equivalent potential vorticity is conserved; this follows from Ertel's theorem and conservation of θ_e:

$$\frac{dq_e}{dT} = 0,$$

$$\text{where} \quad q_e = \zeta(\partial\theta_e/\partial Z)\rho. \tag{4}$$

In the region of ascent it will be assumed that slantwise convection has established a small constant value for q_e as suggested by the observations described in E85. Thus q_e will be held constant for the integration. The source term S is simply related to the rate of change of specific humidity r following the motion:

$$S = -\frac{L}{C_p}\frac{dr}{dT}.$$

It is assumed that the major contribution to the change in r is due to vertical advection along M surfaces, enabling the above expression to be simplified to:

$$S \approx \frac{L}{C_p}\frac{\zeta}{\rho f}\frac{\partial\psi}{\partial X}\frac{\partial r}{\partial Z}. \tag{5}$$

However, an expression for the vertical gradient of r can be obtained in terms of potential vorticity by exploiting the definition of θ_e and equation (4):

$$q_e = \frac{\zeta}{\rho}\frac{\partial}{\partial Z}\left(\theta + \frac{Lr}{C_p}\right) = q + \frac{L}{C_p}\frac{\zeta}{\rho}\frac{\partial r}{\partial Z},$$

or

$$\frac{L}{C_p}\frac{\zeta}{\rho}\frac{\partial r}{\partial Z} = q_e - q. \tag{6}$$

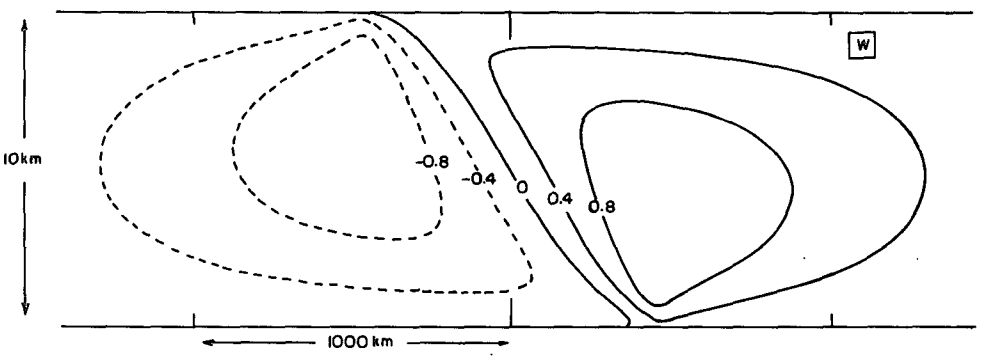

FIG. 2d. As in Fig. 1d but after 1 day of the dry simulation; $w_{max} = 1.1$ cm s^{-1}; $w_{min} = -1.1$ cm s^{-1}.

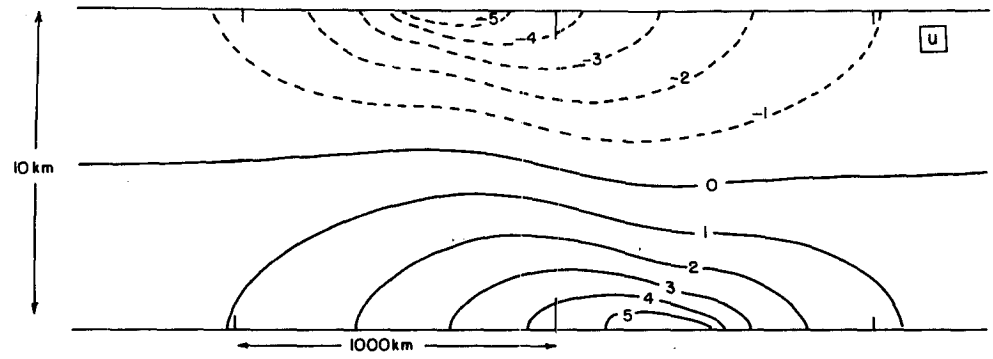

FIG. 2e. As in Fig. 1e but after 1 day of the dry simulation; $u_{a\max} = 5.8$ m s^{-1}; $u_{a\min} = -5.8$ m s^{-1}.

The latent heating should only occur for ascending parcels, assuming that there is little evaporation in the descent region (i.e., that the condensed water appears immediately as rain at the surface). Thus the source term can finally be written as:

$$S = (q - q_e)\left(\frac{w^* + |w^*|}{2}\right), \tag{7}$$

where $w^* = wf/\zeta = -\partial\psi/\partial X$ is the transformed ageostrophic vertical velocity. This concise form for S leads to a simplification in the form of the circulation equation (2):

$$\rho\frac{\partial}{\partial Z}\left(\frac{1}{\rho}\frac{\partial\psi}{\partial Z}\right) + \frac{\partial}{\partial X}\left(\rho\tilde{q}\frac{g}{\theta_0 f^3}\frac{\partial\psi}{\partial X}\right) = -2Q, \tag{8}$$

where

$$\tilde{q} \equiv q_e, \quad \text{if} \quad w > 0,$$

$$\tilde{q} \equiv q, \quad \text{if} \quad w \leq 0.$$

We note that $\tilde{q}$ in (8) plays the same role as static stability does in the quasi-geostrophic form of the Sawyer–Eliassen equation. One may think of $\tilde{q}$ as measure of the resistance to displacements along M-surfaces; it is small for upward displacements of saturated air and large for downward unsaturated displacements. It is apparent now that the equation becomes parabolic for exact neutrality to slantwise convection, hyperbolic if the atmosphere is unstable to slantwise convection, and remains elliptic in the present case of small stability. As shown by E85, the semi-geostrophic approximation breaks down on the approach to neutrality, and it is therefore of interest to determine how small we may make $\tilde{q}$ in these simulations without violating the geostrophic momentum approximation. The equations break down because of the neglect of the inertia of the ageostrophic flow when [see Eq. (17) of E85]:

$$q_e < V_z^2\frac{\theta_0}{g}\zeta\frac{\alpha^2}{f^2}.$$

For the simulation to be described, this corresponds to the following value for the dry frontogenesis solution at $T = 1$ day:

$$q_e < 1.3 \times 10^{-8} \text{ m}^2 \text{ s}^{-1} \text{ K kg}^{-1},$$

or

$$q_e < \frac{1}{20}\, q|_{T=0}.$$

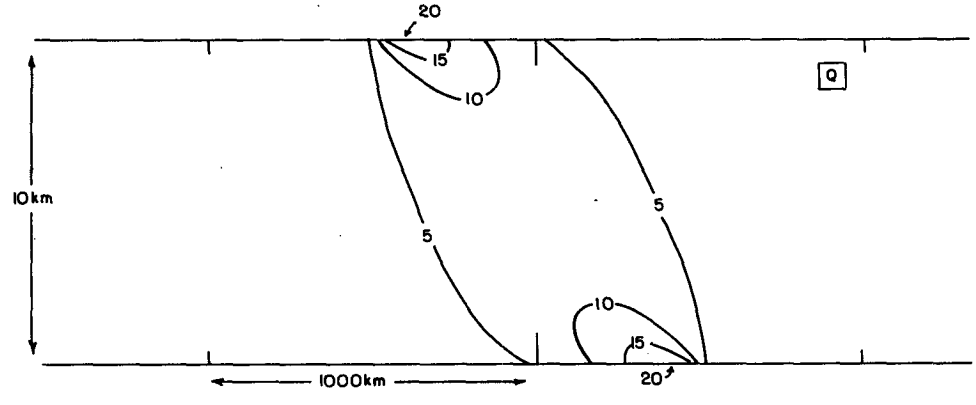

FIG. 2f. As in Fig. 1f but after 1 day of the dry simulation; $Q_{\max} = 2 \times 10^{-3}$ kg m^{-3} s^{-1}.

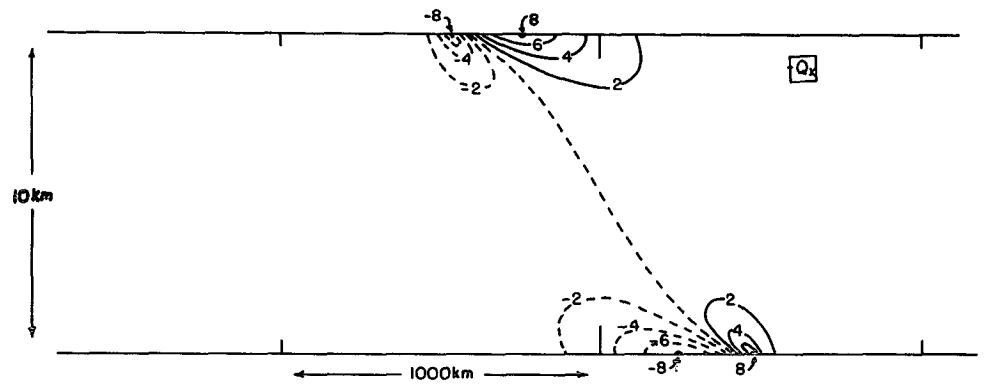

FIG. 2g. As in Fig. 1g but after 1 day of the dry simulation; $-Q_{x\max} = 8.1 \times 10^{-9}$ kg m^{-4} s^{-1}; $-Q_{x\min} = -8.1 \times 10^{9}$ kg m^{-4} s^{-1}.

Including the diabatic term in the potential vorticity equation leads to the following form:

$$\frac{dq}{dT} = \frac{1}{2\rho}\zeta\frac{\partial}{\partial Z}[(q - q_e)(w^* + |w^*|)]. \qquad (9)$$

The elliptic equation for the potential function has no explicit reference to the diabatic term but, of course, q changes in response to the heating.

3. Scale analysis

There are some deductions that can be made about the role of condensation by examination of the form of these equations. In particular, the streamfunction Eq. (8) shows that, in the absence of condensation, ψ is symmetric about $z = H/2$ since the geostrophic forcing Q is symmetric. (Note that the vertical velocity is asymmetric due to the concentration of vorticity at the boundaries.) With condensation, as shown later, Q is very close to being symmetric because the maximum values on the boundaries are unaffected by the diabatic forcing. Hence ψ is very nearly symmetric about $z = H/2$ and so the diabatic source S develops a secondary maximum near the maximum in potential vorticity [see Eq. (7)]. From the prognostic equation (9) for potential vorticity it is clear that this maximum in q will occur toward the lower boundary where the vorticity is a maximum.

From a simple scale analysis of the circulation equation in geostrophic coordinates, it is possible to predict that the ratio of horizontal to vertical scales of the motion is $(\rho q g/\theta_0 f^3)^{1/2}$. If the vertical scale of the motion is the depth of the layer, then it is possible to write the horizontal scale l as:

$$l \sim (\tilde{q}/q_0)^{1/2} L_R, \qquad (10)$$

where $L_R = NH/f$ is the Rossby radius of deformation ($\approx$1000 km in midlatitudes).

Hence, in the descent region, $l \approx L_R$, whereas in the ascent region $l \approx (q_e/q_0)^{1/2} L_R$ which, in the limit described earlier using $q_e = 0.05 q_0$, predicts $l = 220$ km. (In physical coordinates, these scales will be expanded or contracted according to whether the relative vorticity is anticyclonic or cyclonic.)

Using similar arguments, the following scalings apply:

$$\psi \sim H^2 Q, \quad w \sim \frac{\zeta}{\rho f}\frac{H^2 Q}{(\tilde{q}/q_0)^{1/2} L_R}.$$

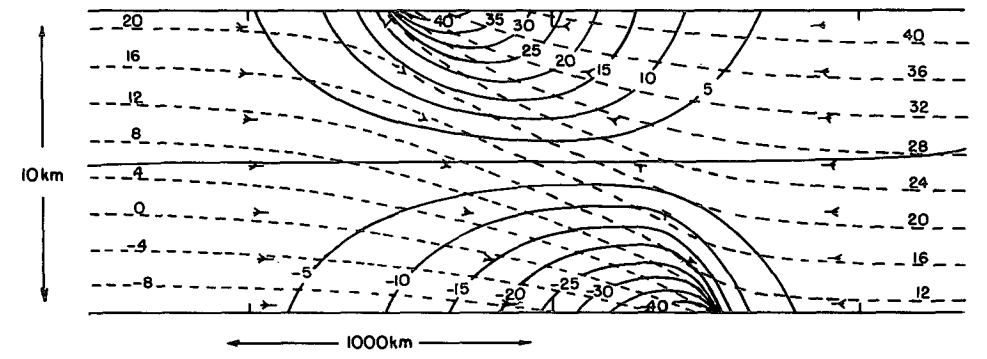

FIG. 3a. As in Fig. 2a but after 1 day of the moist simulation; $V_{\max} = 45.2$ m s^{-1}; $V_{\min} = -45.1$ m s^{-1}.

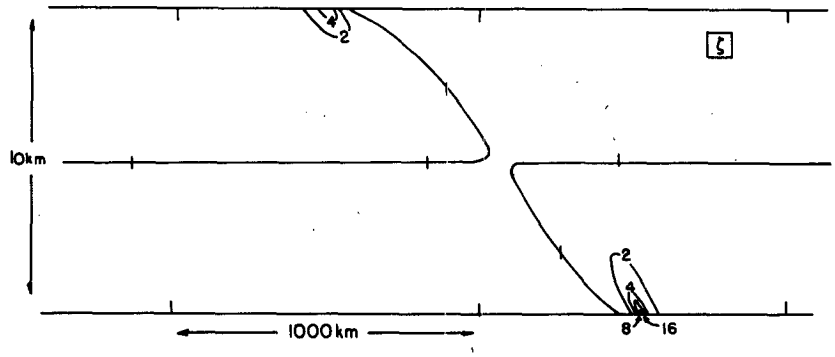

FIG. 3b. As in Fig. 2b but after 1 day of the moist simulation; $\zeta_{max} = 26.4 \times 10^{-4}$ s^{-1}; $\zeta_{min} = 0.5 \times 10^{-4}$ s^{-1}. Note nonuniform contour interval.

Thus, for a given absolute vorticity, the vertical velocity increases with decreasing stability to slantwise convection, while the circulation as given by the amplitude of ψ is relatively constant.

Examination of the vorticity equation with the scalings previously described allows a prediction of the time taken to produce infinite vorticity (frontal collapse) after the relative vorticity has reached f. This can be shown to be:

$$T_c \approx \left(\frac{gq_e}{\rho\theta_0 f^3}\right)^{1/2} \frac{1}{Q}.$$

For the case to be considered in the next section ($q_e/q_0 = 0.07$), T_c is about one-quarter of the time to collapse for the dry front.

The geostrophic state is determined by the potential function (3), which gives a form for the ratio of scales similar to that of the ageostrohic flow, except that $\tilde{q}$ is replaced by q. As q will change due to the diabatic forcing, it is difficult to predict the horizontal scale involved; but as already mentioned, it will be shown that q increases in the lower troposphere in the warm air implying a modest horizontal scale increase there. Consequently, it might be expected that V decreases in the presence of low stability to slantwise convection.

It is of peripheral interest to examine the effect of such diabatic forcing on the growth of the baroclinic wave in which this frontogenesis is imagined to take place. The Eady problem for this situation is solved in the appendix and the solutions show that the effects of condensation are to decrease the scale (and to increase the growth rate) of the maximum growing wave to that described by Eq. (10). The dispersion relation is otherwise unchanged, however.

4. Frontogenesis simulations

a. Results for $q_e/q_0 = 0.07$

In this section we shall make a comparison between dry and moist frontogenesis. The value for q_e is taken to be the initial value of potential vorticity ($q_0 = 2.67 \times 10^{-7}$ m^2 s^{-1} K kg^{-1}) in the dry case and $q_e = 1.87 \times 10^{-8}$ m^2 s^{-1} K kg^{-1} in the moist case. Clearly the potential vorticity stays constant in the dry case but does not in the moist case. The size of the deformation is set as $\alpha = 10^{-5}$ s^{-1}. In the experiments to be described, the Boussinesq approximation is made by setting the density constant.

Various fields are shown in Fig. 1 at the initial time and Figs. 2 and 3 after one day of frontogenesis. In addition to the standard quantities, we show cross sec-

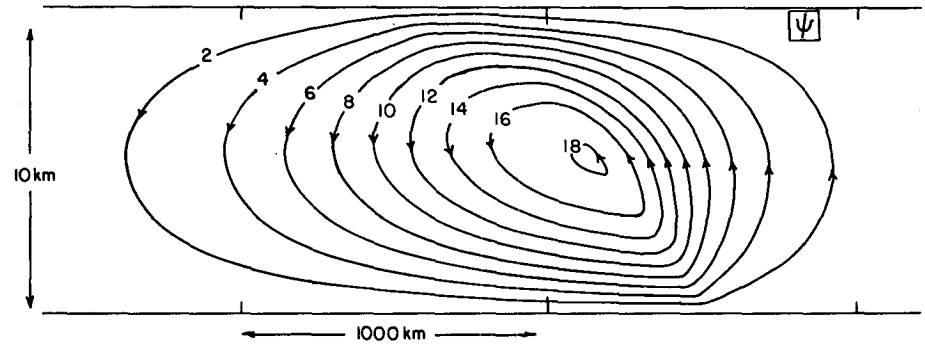

FIG. 3c. As in Fig. 2c but after 1 day of the moist simulation; $\psi_{max} = 18140$ kg m^{-1} s^{-1}.

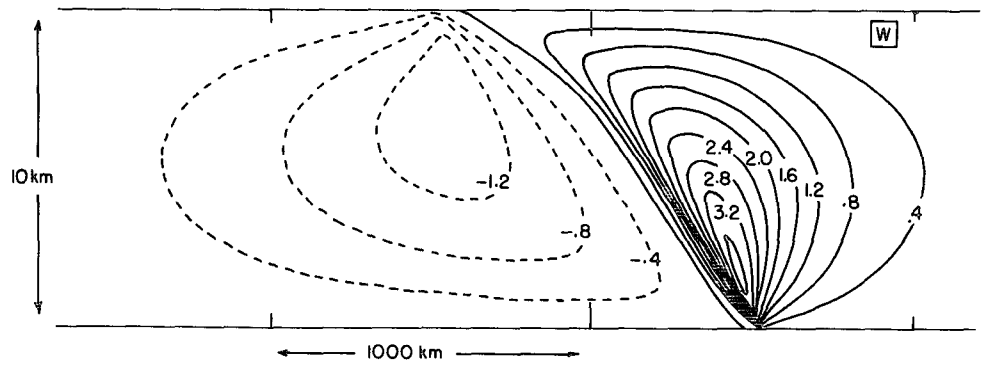

FIG. 3d. As in Fig. 2d but after 1 day of the moist simulation; $w_{max} = 3.7$ cm s^{-1}; $w_{min} = -1.4$ cm s^{-1}.

tions of $-Q_x$ which, for the dry case with constant potential vorticity, is proportional to the forcing of vertical velocity. The figures are reproduced in physical rather than semigeostrophic space.

Figure 1 indicates the fields of interest at the start of both integrations. The moist case was simulated by decreasing q_e smoothly from the initial potential vorticity to 0.07 times that value after one hour, after which it was kept constant.

The dry simulation shown in Fig. 2 indicates that after one day of frontogenesis the relative (cyclonic) vorticity increased from 0.4 to $3.6f$ while the anticyclonic vorticity decreased from -0.28 to $-0.44f$. The front became a discontinuity before 1.5 days. (It should be noted that, due to the choice of the boundary variation in θ, the maximum gradients are at $X = 0$ or $x = x_0 = -V(X = 0)/f$. During the frontogenesis the geostrophic flow at x_0 increases, thus producing a movement of the front toward the warm air. Over the one-day period this represents a translation of 150 km in the dry case.) Other important aspects of the frontogenesis are the vertical symmetry about the midplane and the increase in the geostrophic forcing Q over the period. For this constant potential vorticity case, the transformed vertical velocity $(-\psi_x/\rho)$ is proportional to minus the horizontal gradient of Q (except for boundary effects) and it can be seen that, for example, the zero lines in the $-Q_x$ and w fields are coincident. The vertical velocity maximum has descended from $z = 4.4$ km at $T = 0$ day to $z = 3.6$ km at $T = 1$ day; this is due to w being weighted towards regions of small static stability which, when q is constant, occur where there is large vorticity near the lower boundary. Also, the ageostrophic horizontal velocity is showing the tendency to produce a region of enhanced convergence along the frontal surface.

The moist simulation after one day is shown in Fig. 3. It is clear from the vorticity field that the rate of frontogenesis has been much greater, with maximum relative cyclonic vorticity of $26.4f$. The value is about five times that in the dry case and is consistent with the conclusions from the scale analysis for the time to frontal collapse. However, the minimum vorticity is nearly the same as in the dry case. Vertical symmetry no longer applies; the relative vorticity maximum on the lower boundary is nearly four times that at the upper boundary.

There has been considerable modification of the potential vorticity, with a peak of over five times the initial value at the surface. The region of decrease in q is extensive at upper levels but with a much smaller pointwise change. As we have taken the minimum lifting condensation level to be the surface rather than a more realistic elevated level, the vertical gradient of heating

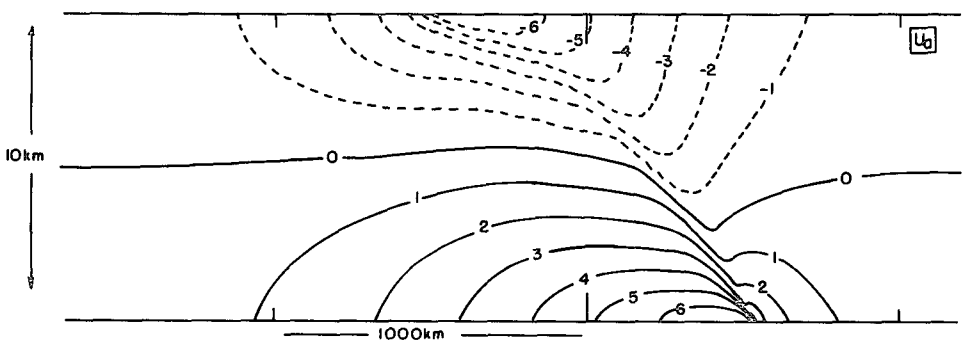

FIG. 3e. As in Fig. 2e but after 1 day of the moist simulation; $u_{amax} = 6.90$ m s^{-1}; $u_{amin} = -6.91$ m s^{-1}.

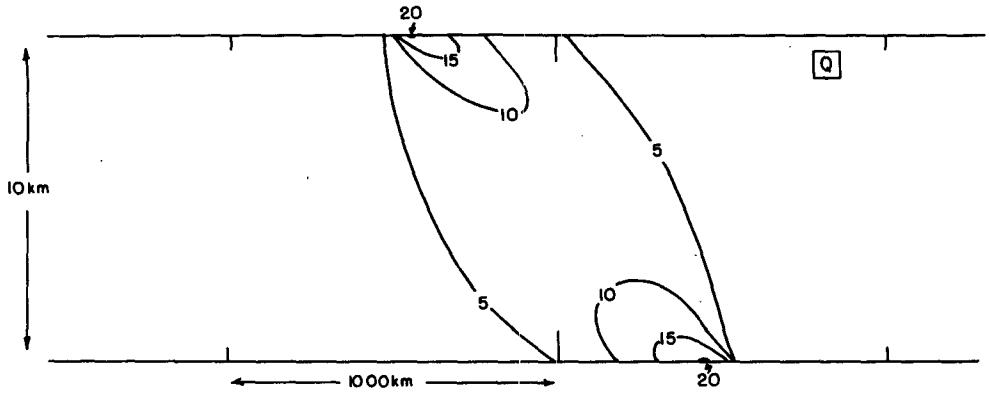

FIG. 3f. As in Fig. 2f but after 1 day of the moist simulation; $Q_{max} = 20 \times 10^{-4}$ kg m^{-3} s^{-1}.

is large at the surface. This produces a maximum potential vorticity which migrates from $z \sim 260$ m after $T \sim 0.5$ day to the surface after 4 days. If a more realistic elevated condensation level had been taken the peak in q would have been near that level. It is apparent that there is now a change of sign in the gradient in q along isentropes, which is the necessary condition for internal baroclinic/barotropic instability in semigeostrophic theory (see Hoskins, 1976). This point will be considered further in the next section.

It is interesting to note that one effect of the low-level increase in potential vorticity is that the geostrophic flow maximum is only increased by 10% despite the 500% increase in vorticity. Thus, at the time a discontinuity forms, the geostrophic flow is less in the moist case than in the dry case. This change due to the effects of moisture allows the geostrophic flow to look more realistic, since the dry frontogenesis structure in two dimensions overestimates the flow.

As predicted by E85 and described in the previous section, the ageostrophic ascent is now on a much smaller horizontal scale. [This scale contraction of the updraft was also found in the work of Williams *et al.* (1981) and Hsie *et al.* (1984), although unstable condensation occurred in these simulations.] The vertical velocity has increased threefold while the horizontal velocity has increased only slightly. The point maximum ascent is now at $z = 1.4$ km and the particle displacements indicate that at low levels there is nearly vertical flow above the surface front. This can be compared favorably with the "jet of strong ascent" described from observations of a cold front by Sanders (1983), and also obtained in numerical simulations by Keyser and Anthes (1982). (In the latter case, the frontal jet of ascent was associated with boundary friction.) A comparison of the vertical velocity field and the geostrophic forcing $-Q_x$ indicates that now there is descent, particularly at midlevels, in a region where there is geostrophic forcing of ascent. The position of the zero-line in vertical velocity is about 90 km ahead of that in $-Q_x$ at midlevels. This can be compared with the prediction made by E85 for this displacement which, given a value of the horizontal scale of Q of 200 km, yields a value of 86 km. However, E85 assumes this displacement is independent of height, which it is not, and in particular it falls to nearly zero (both in physical and geostrophic coordinates) at the boundaries.

From this result E85 goes on to speculate that this descent may lead to an additional frontolytic contribution by the ageostrophic flow compared to the dry

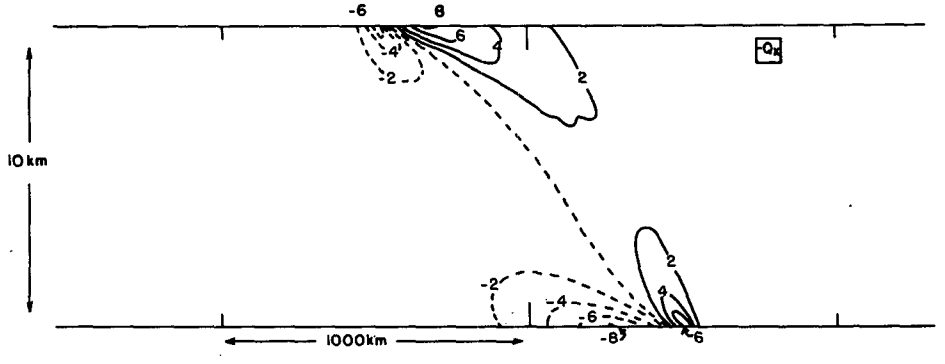

FIG. 3g. As in Fig. 2g but after 1 day of the moist simulation; $-Q_{xmax} = 8.2 \times 10^{-9}$ kg m^{-4} s^{-1}; $-Q_{xmin} = -8.1 \times 10^{-9}$ kg m^{-4} s^{-1}.

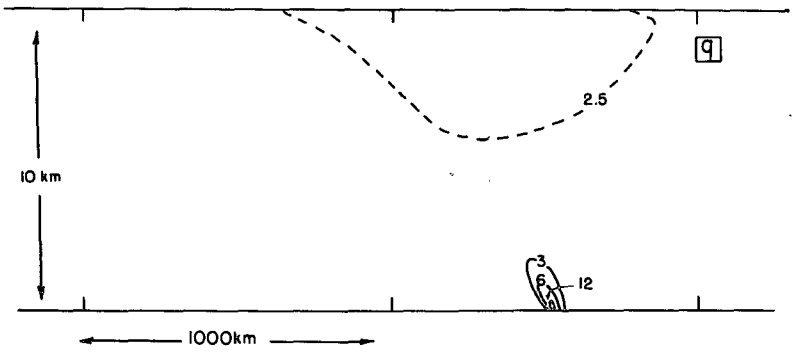

FIG. 3h. Potential vorticity (10^{-7} m^2 K s^{-1} kg^{-1}) after 1 day of the moist simulation. The initial value of q is 2.7×10^{-7} m^2 K s^{-1} kg^{-1}, while the maximum and minimum values are 17.4×10^{-7} m^2 K s^{-1} kg^{-1} and 1.7×10^{-7} m^2 K s^{-1} kg^{-1}, respectively. The dashed line shows the contour enclosing potential vorticity less than 2.5×10^{-7} m^2 K s^{-1} kg^{-1}.

case. The equation for the rate of change of frontogenesis in physical coordinates is given by:

$$\frac{d}{dt}\left(\frac{\theta x^2}{2}\right) = \theta_x\left(\frac{f^2\theta_0}{\rho g}Q - \frac{\partial u}{\partial x}\frac{\partial \theta}{\partial x} - \frac{\partial w}{\partial x}\frac{\partial \theta}{\partial z} + \frac{\partial S}{\partial x}\right). \quad (11)$$

It is clear that near the surface the frontogenesis is due to the first two terms on the right-hand side of this equation. It can be seen from the figures that u has a maximum behind the surface front and so both these terms are frontogenetic at the surface frontal position.

The horizontal ageostrophic flow has a frontal structure itself, with a very sharply defined zone of convergence along the frontal surface at low- and midlevels. This does not appear in the dry solutions. Such a structure would probably be subject to small-scale instabilities, as the local Richardson number minimum is 0.05. It is possible, however, that internal baroclinic/barotropic instability may occur before the Richardson number falls below 0.25, as discussed in the next section.

b. *Results as a function of q_e/q_0*

Other moist simulations were performed varying only the value of q_e/q_0. It is apparent that a square root dependence on (q_e/q_0) is typical for w_{max}, q_{max} and ζ_{max} but, as hypothesized in Section 3, ψ_{max} has only a weak functional dependence. In fact ψ_{max} increases slightly with decreasing q_e but the volume integral of ψ does not vary with (q_e/q_0). This is due, in turn, to the constancy of Q, which is itself a somewhat surprising result given the increasing rate of frontogenesis as q_e decreases. It is clear, therefore, that the additional frontogenesis is due to an increase in the ageostrophic contribution.

5. Discussion

It has been shown that in an atmosphere which has small stability to slantwise convection, frontogenesis proceeds at a much increased rate and the horizontal scale of the ascent in the warm air is considerably reduced. One main conclusion, therefore, is that cross-frontal circulations produced by geostrophic forcing

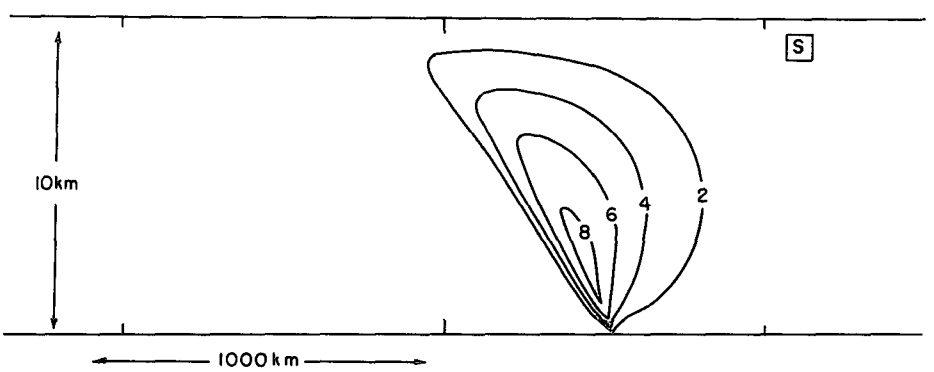

FIG. 3i. Condensation heating at 1 day of the moist simulation. Maximum value is 0.86×10^{-4} K s^{-1}.

are similar in structure to slantwise convection, despite (small) stability to the latter. This is true to the extent that we believe it may be difficult to distinguish frontal from slantwise convective circulations using observations. The appearance of multiple bands in some circumstances suggests that slantwise convection may occur in these cases.

In contrast to previous studies, we have formulated the condensational heating in such a way as to be consistent with the observed frontal distribution of temperature and moisture, which shows a remarkable tendency toward moist adiabatic conditions along geostrophic momentum surfaces (Emanuel, 1983a, 1985; Sanders and Bosart, 1985). This condition is also implied by the theory of slantwise convection, which suggests that the adjustment time is short compared to the time scale typical of evolving baroclinic waves. The present study has not addressed the problem of just how the slantwise convection, in the presence of frontogenetical forcing, achieves a state of near neutrality to the convection. A numerical approach to this problem is necessary in which, unlike in the present model, the slantwise convection can be explicitly represented along with the geostrophic forcing necessary to produce frontogenesis. Such a model must solve the primitive equations, as the assumption of semigeostrophy filters out slantwise (and upright) convective motion.

It is apparent that one of the most important effects of diabatic processes at fronts is the generation of sources and sinks of potential vorticity. In particular, this study has shown that if a baroclinic wave grows and develops fronts in an environment of initially constant potential vorticity, condensation will cause a strong local maximum in q at low levels. Baroclinic instability, as envisaged in the Eady problem, develops in an atmosphere with constant q in the interior but with a horizontal temperature gradient at the boundaries. As such it satisfies the necessary conditions for instability described by Charney and Stern (1962), i.e., that there be a maximum or minimum in q and/or a non-zero temperature gradient at the boundary. In fact, it is possible to describe such a temperature gradient at the boundary as a delta function in potential vorticity which itself represents an extremum of q. The extra ingredient of an interior maximum in q produced by the condensation raises the possibility that, superimposed on the baroclinic instability leading to the frontogenesis itself, there may be a secondary internal baroclinic/barotropic instability. This would probably produce a maximum growing wave on the horizontal scale of either the horizontal variation of q or the local Rossby radius of deformation given by the expression Nh/f, where h is the height scale of the variation in potential vorticity (and of the ensuing instability) and N is the local Brunt–Väisälä frequency. For a plausible lifting condensation level of 1 km, where the peak in potential vorticity might be expected, and $N = 0.8 \times 10^{-2}$ s^{-1} we estimate a horizontal scale of about 80 km. This instability would be manifest by a wave of this horizontal scale in the along-front direction. Waves of this character have been observed at many fronts (Parsons and Hobbs, 1983) and a multiple Doppler analysis of a wavy front by Carbone (1982) clearly shows the waves developing along a shear line of concentrated vorticity. Parsons and Hobbs (1983) speculated that the waves were due to barotropic instability; we would generalize that speculation to one pertaining to internal baroclinic/barotropic instability. The present results suggest that condensation is very effective in creating a local, line-symmetric extremum in potential vorticity. In a highly baroclinic environment such as a front it is not sufficient to assess dynamical stability purely on the grounds of vorticity gradients. For example, the dry frontogenesis problem described in this paper produces strong geostrophic vorticity gradients which are stable, however, since the potential vorticity is constant. The further investigation of this internal instability requires use of a three-dimensional numerical model; this problem seems worthy of further research. It is likely that such an instability would grow before the front has collapsed to a scale at which Kelvin–Helmholtz type instabilities set in due to the large vertical shears.

We believe that in order for problems like these to be understood more fully, it is necessary to obtain better mesoscale observations in the vicinity of fronts. Observational programs should necessarily concentrate on the dynamical structure of such systems and specifically attempt to test some of the theoretical concepts developed in this and other research. In order to resolve the thermodynamic details of the frontal zone, a facility such as a dropsonde system capable of making a sounding every 30–50 km would be necessary, while Doppler radar would enable even more kinematic detail to be obtained. In attempting to understand both frontal circulations and slantwise convection, it is crucial to obtain accurate measurements of the geostrophic flow in and around the frontal zone, and this requires excellent thermodynamic data. This important point should be borne in mind in the design of field experiments concerned with these phenomena.

Acknowledgments. The authors would like to acknowledge receipt of NATO Grant 129/84 for the collaboration necessary to complete this work. K. Emanuel was supported in part by National Science Foundation Grant ATM-8313454. Use of the two-dimensional semigeostrophic numerical model developed by Professor B. J. Hoskins, Dr. W. H. Heckley and Mr. E. Caetano is gratefully acknowleged.

APPENDIX

The Semigeostrophic Eady Model of Baroclinic Instability Including Diabatic Forcing

As shown by Hoskins (1976), the equations described in Section 2 can be used to obtain the semigeostrophic

version of the Eady problem for baroclinic instability. The solution is shown to be identical with the quasi-geostrophic Eady wave except that it is oriented along the absolute vorticity vector lines. Also, the semigeostrophic formulation allows the nonlinear wave development to be simulated numerically, which cannot be done consistently using the quasi-geostrophic equations. It is the intention here to include the diabatic forcing consistent with small stability to slantwise convection in the linear Eady problem. This is relatively simple using semigeostrophic equations, but not so in the quasi-geostrophic case.

The Eady wave problem consists of examining the stability of a constant vertical shear zonal flow to three-dimensional perturbations. Hence $V = \bar{V}_z Z$ where $\bar{V}_z$ is a constant and the potential vorticity equation (1) can be linearized to give:

$$\left(\frac{\partial}{\partial T} + \bar{V}_z Z \frac{\partial}{\partial Y}\right) q' + u' \frac{\partial \bar{q}}{\partial X} + w' \frac{\partial \bar{q}}{\partial Z} = -\frac{\partial}{\partial Z}[(q_e - \bar{q})w']. \quad \text{(A1)}$$

Here we have used the diabatic forcing term derived in Section 2 and given in (7). In (A1), an overbar indicates the basic state and a prime the perturbation. As we will seek wave solutions to this equation, it is not possible, unlike the frontogenesis simulations described in Section 4, to prevent diabatic forcing for descending parcels. This unrealistic aspect is typical of linear analyses including convective processes and it limits the applicability of the results to the atmosphere. The conclusions from this analysis at least indicate the tendency, if not the detail, of the development of the Eady wave in conditions of small stability to slantwise convection.

As described in Hoskins (1976), to obtain an expression for $\bar{q}$ and q' a linearization has to be performed of the three-dimensional form of equation (3). Furthermore, with the constant shear basic state it should be noted that $\bar{\zeta} = f$, $\bar{q}_x = 0$, and $\bar{q}_z = 0$. An expression for w' is obtained from the linearized thermodynamic equation:

$$\left(\frac{\partial}{\partial T} + \bar{V}_z Z \frac{\partial}{\partial Y}\right) \theta' + u' \frac{\partial \bar{\theta}}{\partial X} + w' \frac{\partial \bar{\theta}}{\partial Z} = \frac{-\rho w'}{f}(q_e - \bar{q}). \quad \text{(A2)}$$

Using the thermal wind relationship, the definitions of θ in terms of Φ and $u' = -\Phi'_y/f$ an expression for w' can be found; substituting into equation (A2) gives:

$$\left(\frac{\partial}{\partial T} + \bar{V}_z Z \frac{\partial}{\partial Y}\right)\left[\Phi'_{zz} + \frac{g\rho q_e}{\theta_0 f^3}(\Phi'_{xx} + \Phi'_{yy})\right] = 0. \quad \text{(A3)}$$

The boundary conditions are obtained by assuming rigid horizontal boundaries at $Z = 0, H$ where $w' = 0$. Thus:

$$\left(\frac{\partial}{\partial T} + \bar{V}_z Z \frac{\partial}{\partial Y}\right)\Phi'_z = \bar{V}_z \Phi'_y \quad \text{on} \quad Z = 0, H. \quad \text{(A4)}$$

It can be seen that the eigenvalue problem specified by (A3) and (A4) is identical with that for the dry Eady problem except that q is replaced by q_e in (A3). Therefore, q_e plays the role of a reduced static stability in the semigeostrophic formulation. Hence, assuming wave-like solutions of the form $\Phi = f(z)\exp[i(k_x X + k_y Y) + \sigma T]$ leads to the following dispersion relation:

$$\frac{\sigma}{\bar{V}_z} = \frac{-k_y H}{2} \times \{1 \pm [1 - 4(\nu_m H \coth(\nu_m H) - 1)/(\nu_m H)^2]^{1/2}\},$$

where

$$\nu_m \equiv \left[\frac{g\rho q_e}{\theta_0 f^3}(k_x^2 + k_y^2)\right]^{1/2}.$$

This expression for the vertical wavenumber can be rewritten in terms of that for the dry problem:

$$\nu_m = \nu_d (q_e/\bar{q})^{1/2},$$

where m and d refer to the moist and dry cases, respectively. Thus, this result is in accord with that described in Section 3 for the ratio of the vertical to horizontal scales of the motion.

For the most unstable wave $k_x = 0$ the quantity $(g\rho q_e/\theta_0 f^3)^{1/2}\sigma/\bar{V}_z$ has the same functional dependence on ν as it has in the dry problem when q_e is replaced by q; i.e.,

$$\text{maximum growth rate} \quad \sigma_m = \sigma_d(\bar{q}/q_e)^{1/2} \quad \text{at} \quad \nu_d H = 1.602(\bar{q}/q_e)^{1/2},$$

$$\text{short wave cutoff at} \quad \nu_d H = 2.4(\bar{q}/q_e)^{1/2}.$$

Thus the effect of decreasing the stability to slantwise convection is to increase the wavenumbers of the wave of maximum growth rate and the short wave cutoff while increasing the maximum growth rate. As an example, assume $q_e/\bar{q} = 0.5$ in which case the ratios of the wavelength and growth rate of the maximum growing wave in the moist and dry case are given by:

$$L_m/L_d = 0.71, \quad (L_m \approx 2785 \text{ km})$$

$$\sigma_m/\sigma_d = 1.41.$$

These results are reminiscent of those of Mak (1982), (see Fig. 1 of that paper), who considered an approach to this problem using quasi-geostrophic theory. A crucial distinction is that in the current formulation it is the effects of slantwise convection that are being accounted for while Mak (1982) considered all processes leading to condensational heating. The condensational heating used here invokes the known conservation of equivalent potential vorticity, while that used in Mak (1982) is dependent on boundary layer moisture convergence, independent of the atmospheric stability. As

the (arbitrary) heating amplitude in the Mak (1982) formulation increases, eventually the tendency to increase the growth of the wave is reversed. This result is perplexing and is probably due to the physically obscure partitioning of the heating between the rotational and divergent components of the flow. The point has been made here and by Emanuel (1985) that the semigeostrophic equations break down for small q_e and so it is not consistent to use such results for large diabatic forcing. It is likely that the maximum in growth rate as a function of the heating amplitude quoted by Mak (1982) occurs only after the quasi-geostrophic equations are similarly invalid.

It is of great interest, therefore, to attempt a nonlinear simulation of baroclinic instability using semigeostrophic equations including the nonlinearity of the diabatic forcing, which unfortunately cannot be allowed for in the linear problem. This will be the subject of future research.

REFERENCES

Bennetts, D. A., and B. J. Hoskins, 1979: Conditional symmetric instability—A possible explanation for frontal rainbands. *Quart. J. Roy. Meteor. Soc.*, **105,** 945–962.

Betts, A. K., 1983: Atmospheric convective structure and a convection scheme based on saturation point adjustment. *ECMWF Proc.* Workshop on Convection in large-scale models. 69–94.

Carbone, R. E., 1982: A severe frontal rainband. Part I: Stormwide hydrodynamic structure. *J. Atmos. Sci.*, **39,** 258–279.

Charney, J. G., and M. E. Stern, 1962: On the stability of internal baroclinic jets in a rotating atmosphere. *J. Atmos. Sci.*, **19,** 159–171.

Emanuel, K. A., 1983a: On assessing local conditional symmetric instability from atmospheric soundings. *Mon. Wea. Rev.*, **111,** 2016–2033.

——, 1983b: The Lagrangian parcel dynamics of moist symmetric instability. *J. Atmos. Sci.*, **40,** 2369–2376.

——, 1985 (E85): Frontal circulations in the presence of small moist symmetric stability. *J. Atmos. Sci.*, **42,** 1062–1071.

Heckley, W. H., 1980: Frontogenesis. Ph.D. thesis, University of Reading, 209 pp.

Hoskins, B. J., 1976: Baroclinic waves and frontogenesis. Part I: Introduction and Eady waves. *Quart. J. Roy. Meteor. Soc.*, **102,** 103–122.

——, 1982: The mathematical theory of frontogenesis. *Annual Reviews in Fluid Mechanics,* Annual Reviews, **14,** 131–151.

——, and F. P. Bretherton, 1972: Atmospheric frontogenesis models: Mathematical formulation and solution. *J. Atmos. Sci.*, **29,** 11–37.

Hsie, E.-Y., R. A. Anthes and D. Keyser, 1984: Numerical simulation of frontogenesis in a moist atmosphere. *J. Atmos. Sci.*, **41,** 2581–2594.

Keyser, D., and R. A. Anthes, 1982: The influence of planetary boundary layer physics on frontal structure in the Hoskins-Bretherton horizontal shear model. *J. Atmos. Sci.*, **39,** 1783–1802.

Mak, M., 1982: On moist quasi-geostrophic baroclinic instability. *J. Atmos. Sci.*, **39,** 2028–2037.

Parsons, D. B., and P. V. Hobbs, 1983: The mesoscale and microscale structure and organization of clouds and precipitation in midlatitude cyclones. XI: Comparisons between observational and theoretical aspects of rainbands. *J. Atmos. Sci.*, **40,** 2377–2397.

Ross, B. B., and I. Orlanski, 1978: The circulation associated with a cold front. Part II: Moist case. *J. Atmos. Sci.*, **35,** 445–465.

Sanders, F., 1983: Observations of fronts. *Mesoscale meteorology—Theories, observations, and models,* D. Reidel, pp. 175–204.

——, and L. F. Bosart, 1985: Mesoscale structure in the megalopolitan snowstorm of 11–12 February 1983, Part I: Frontogenetical forcing and symmetric instability. *J. Atmos. Sci.*, **42,** 1050–1061.

Sawyer, J. S., 1956: The vertical circulation at meteorological fronts and its relation to frontogenesis. *Proc. Roy. Soc. London,* **A234,** 346–362.

Sundqvist, H., 1978: A parameterization scheme for non-convective condensation including prediction of cloud water content. *Quart. J. Roy. Meteor. Soc.*, **104,** 677–690.

Thorpe, A. J., and C. A. Nash, 1984: Convective and boundary layer parameterizations in a diagnostic model of atmospheric fronts. *Quart. J. Roy. Meteor. Soc.*, **110,** 443–466.

Williams, R. T., L. C. Chou and C. J. Cornelius, 1981: Effects of condensation and surface motion on the structure of steady-state fronts. *J. Atmos. Sci.*, **38,** 2365–2376.